Microfluidic encapsulation of SN-38 in block copolymer nanoparticles: effect of hydrophobic block composition on loading and release properties

Danica Jensen, Yimeng Cao, Changhai Lu, Jeremy E. Wulff, & Matthew G. Moffitt

January 2019

Microfluidic Encapsulation of SN-38 in Block Copolymer Nanoparticles: Effect of Hydrophobic Block Composition on Loading and Release Properties

Danica Jensen; Yimeng Cao; Changhai Lu; Jeremy E. Wulff and Matthew G. Moffitt*

Department of Chemistry, University of Victoria, P.O. Box 1700, Victoria, BC, Canada V8W 3V6

* E-mail: mmoffitt@uvic.ca

Tel.: (250) 721-7162

Fax: (250) 721-7147

Abstract

A gas-liquid microfluidic reactor was used to prepare polymer nanoparticles (PNPs) containing the drug 7-ethyl-10-hydroxy camptothecin (SN-38) from a series of poly(methyl caprolactone-*co*-caprolactone)-*b*-poly(ethylene oxide) (P(MCL-*co*-CL)-*b*-PEO) amphiphilic block copolymers with variable MCL content in the hydrophobic block. All three copolymers formed spheres with ~20-nm core diameters by TEM although some rigid rodlike aggregates were also formed by the PMCL-50 and PMCL-75 copolymers. SN-38 encapsulation efficiencies (*EE* = 2.7-3.0%) and loading levels (*DL* = 2.0-2.9%) were similar for the three copolymers. *In vitro* release kinetics became significantly slower as the MCL content increased, with release half times increasing monotonically from 3.4 to 6.2 h as the MCL content of the hydrophobic block increased from 50% to 100%. The ability to systematically tune release half times *via* controlled variation in the hydrophobic block composition, while maintaining constant PNP size and loading levels, represents an intriguing chemical handle for the optimization of SN-38 nanomedicines.

Key Words: Drug Delivery, Cancer Therapy, Block Copolymers, Microfluidics, Micelles

Graphical Abstract:

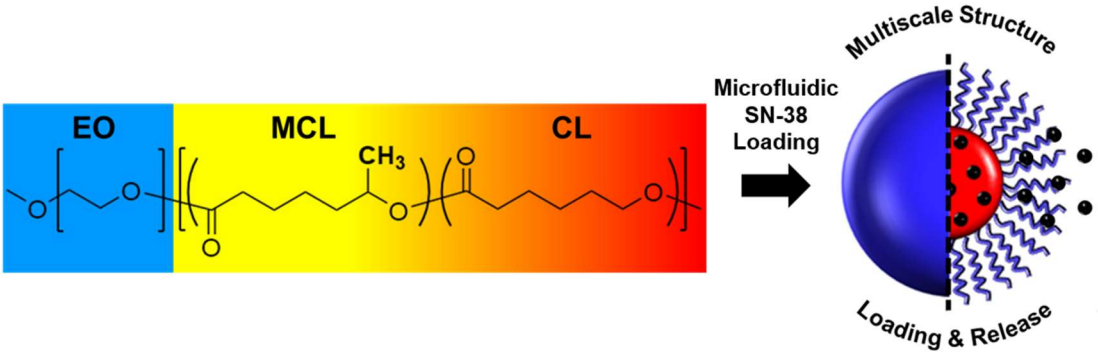

Introduction

The drug 7-ethyl-10-hydroxy camptothecin, or SN-38, is a promising anticancer agent, and *in vitro* cytotoxicity assays show that it can be effective against ovarian, lung and colorectal cancers. SN-38 is a synthetic analog of camptothecin, and like camptothecin shows activity as a DNA topoisomerase inhibitor.[1] The active form of SN-38 consists of a five-ring structure, with the terminal ring comprising an alpha-hydroxylactone structure which is formed at low pH (< 4.5). At pH > 9 this ring is completely hydrolyzed to the carboxylate form, which has no therapeutic benefits. This presents a challenge for clinical use, as the open-ring carboxylate structure is the favoured form of SN-38 at physiological pH. Another challenge is the insolubility of SN-38 in water and other pharmaceutically relevant solvents, making it difficult to deliver the drug through typical methods. For this reason, SN-38 is currently administered in the form of the prodrug irinotecan (Captosar®, Pfizer), which is converted by carboxylesterases in the liver. Irinotecan is soluble in water, but pharmacological data show that it is between 100- and 1000-fold less effective than SN-38.[1, 2]

Accumulation of macromolecules and nanoparticles in the size range of 50-100 nm in tumour tissue due leaky tumour vasculature is termed the enhanced permeability and retention (EPR) effect, and has been applied to increase drug specificity and decrease the required dose of administered drug.[3] Encapsulating SN-38 in a polymer nanoparticle (PNP) takes advantage of the EPR effect to target drug delivery toward tumour tissues.[1, 4-13] Amphiphilic block copolymers spontaneously form micellar PNPs with a hydrophilic external corona and a hydrophobic internal core. The SN-38 can be contained within the water-dispersible PNPs, which travel to target tissues through the circulatory system. Various polymer types have been researched to optimize SN-38 delivery, including those with hydrophobic blocks comprised of poly(lactic-*co*-glycolic acid)

(PLGA),[12] polygluamate (PGlu),[4-6] and poly(ε-caprolactone) (PCL).[8, 11, 13] Poly(ε-caprolactone)-*b*-poly(ethylene oxide) (PCL-*b*-PEO) is a commonly applied amphiphilic block copolymer in drug delivery investigations, due to the biodegradable and biocompatible nature of its component blocks.[14] Although the hydrolytic degradation of PCL makes it an appropriate *in vivo* host for a wide variety therapeutic molecules, its semicrystalline nature can strongly influence drug delivery properties.[15, 16] For example, an increase in the crystallinity of the core-forming PCL blocks has been shown to increase drug release times in some studies.[15-18] However, crystallites can also exclude drug molecules leading to lower encapsulation efficiencies.[15, 16, 18] In addition, SN-38 generally shows low solubility in aliphatic polyesters including PCL and PLGA.[11] Together these features highlight a need for studies involving systematic variation in block copolymer hydrophobic block composition and crystallinity, in order to gain insights *en route* to improved materials for SN-38 delivery systems.

In a recent paper, we described the synthesis and self-assembly of a series of biocompatible poly(methyl caprolactone-*co*-caprolactone)-*b*-poly(ethylene oxide) (P(MCL-*co*-CL)-*b*-PEO) amphiphilic block copolymers with variable MCL content in the hydrophobic block.[19] The MCL monomer possesses a methyl group that disrupts polymer crystallization, such that its incorporation within the hydrophobic block offers chemical tunability of the structure and properties of the PNP core for drug delivery. We showed that self-assembly gives rise to PNPs with hydrophobic cores that decrease in crystallinity as the MCL content increases, while morphologies and PNP sizes showed non-monotonic trends with MCL content. Moreover, we demonstrated that PNPs loaded with another common anticancer drug, paclitaxel (PAX), gave rise to slower PAX release and more potent antiproliferation effects against MCF-7 breast cancer cells as the MCL content increased.[19]

In this study, we apply the same series of P(MCL-*co*-CL)-*b*-PEO copolymers described in ref. 19 to investigate the effect of the hydrophobic block composition on the encapsulation and release of SN-38 from the resulting SN-38-loaded PNPs (SN-38-PNPs). Three different block copolymers are applied with MCL contents relative to the total hydrophobic block weight of 50 wt %, 75 wt % and 100 wt %, designated PMCL-50, PMCL-75, and PMCL-100, respectively. All SN-38-PNPs are manufactured using a two-phase gas-liquid microfluidic reactor, which has been described previously by our group.[15, 16, 18-28] An interesting feature of this reactor are the high-shear "hot spots" in the corners of the liquid plugs which provide flow-variable processing of PNPs downstream of water/copolymer mixing and the resulting self-assembly. In previous work, we demonstrated that changes in the manufacturing flow rate within the microfluidic channels allow the maximum shear rate to be varied,[28] enabling shear processing control of sizes,[20, 21] morphologies,[15, 22] and drug delivery properties[15, 16, 18, 19, 26] of various PNP materials. However, the objective of this study is to investigate the chemical effects of the hydrophobic block composition, independent of flow effects, and so all microfluidic SN-38-PNP preparations are performed at the same nominal flow rate.

Experimental

Materials. The three copolymers PMCL-50, PMCL-75, and PMCL-100 (Table 1) were synthesized and characterized in our lab, as described in detail in ref. 19. Briefly, all three copolymers are poly(methyl caprolactone-*co*-caprolactone)-*block*-poly(ethylene oxide) (P(MCL-*co*-CL)$_{5k}$-*b*-PEO$_{5k}$) block copolymers in which the hydrophobic core-forming block is a random copolymer consisting of various relative amounts of MCL and CL monomers, and the subscripts refer to the number-average molecular weights of the corresponding blocks. The numbers designating the three different copolymers in the series refer to the weight percentages of MCL

monomer relative to the total weight of MCL and CL monomers in the hydrophobic block. For example, PMCL-75 possesses a hydrophobic block comprised of 75 wt % MCL and 25 wt % CL. Reliable M_n values could not be obtained using GPC with RI and LALS detectors, possibly due to the weak light scattering from shorter PCL chains in the distribution within the mobile THF phase. Therefore, we combined M_n values determined from NMR with M_w values determined from GPC to calculate the dispersity values $Đ$ reported in Table 1. Reported critical water contents (cwc) for each of the copolymers in 0.33 wt % solutions in DMF were determined as described in ref. 19. These values represent the water content in the microfluidic channels above which the hydrophobic blocks will undergo microphase separation to form PNPs. The on-chip water content for PNP formation for each of the three copolymers is selected to be the same relative to the critical water content: cwc + 10 wt %.

Table 1. Copolymer Characteristics and Critical Water Contents (cwc).

Copolymer	M_n P(MCL-*co*-CL)-*b*-PEO[a]	M_n P(MCL-*co*-CL)	f_{MCL}	$Đ$[b]	cwc / wt %[c]
PMCL-50	9795	4795	0.49	1.95	8.8 ± 0.1
PMCL-75	9432	4432	0.72	1.77	9.4 ± 0.3
PMCL-100	9690	4690	1	2.34	9.3 ± 0.2

a) M_n(PEO) = 5000 g/mol.

b) $Đ = M_w$(GPC)/M_n(NMR).

c) Errors are standard deviations of three separate cwc measurements.

7-ethyl-10-hydroxycamptothecin (SN-38) was purchased from AK Scientific (≥ 98.0%). NaCl (Bio Basic Canada, 99.9%), KCl (Caledon, 99.0%), Na_2HPO_4 (BioBasic Canada, 98.0%) and KH_2PO_4 (Caledon, 99.0%) were used to prepare phosphate buffered saline (PBS, pH = 7.4). *N*,*N*-dimethylformamide (DMF, Caledon, 99.8%) and acetonitrile (Caledon, HPLC grade) were used as received without further purification.

Microfluidic Reactor Fabrication. Negative masters were fabricated on silicon wafers (Silicon Materials) using the negative photoresist SU-8 100 (Microchem). A 150 µm-thick SU-8 film was spin-coated at 2000 rpm onto the silicon wafer and heated at 65 °C for 12 min and then at 95 °C for 50 min. After the wafer was cooled, a photomask was placed directly above and the wafer was exposed to UV light for 100 s. Then, the UV-treated film was heated at 65 °C for 1 min and then 95 °C for 20 min. Finally, the silicon wafer was submerged in SU-8 developer (Microchem) and rinsed with isopropanol until all unexposed photoresist was removed.

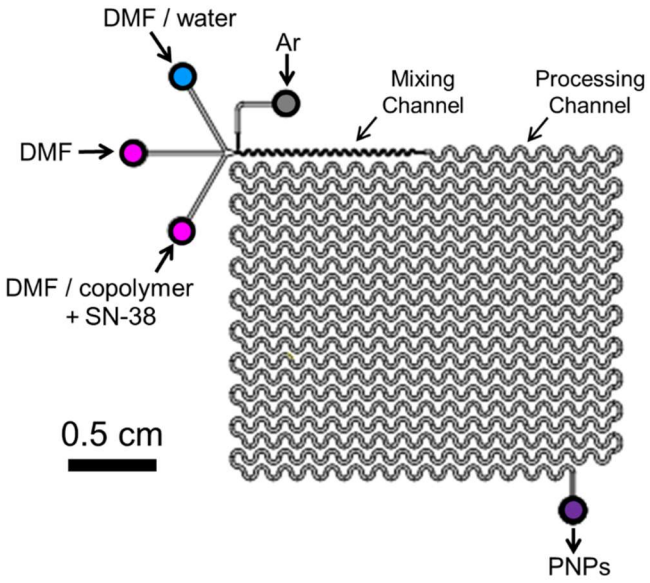

Figure 1. Schematic of two-phase gas-liquid microfluidic reactor. For all experiments, the gas-to-liquid flow ratio was ~1, the nominal on-chip flow rate was Q = 200 µL/min, the on-chip water content was cwc + 10 wt %, and the SN-38/polymer (w/w) loading ratio was r = 0.75.

Microfluidics chips were fabricated from poly(dimethyl siloxane) (PDMS) using a SYLGARD 184 silicon elastomer kit (Dow Corning). For fabrication of all PDMS chips, the elastomer and curing agent were mixed at a 7:1 ratio and degassed under vacuum. The resulting mixture was poured over a clean negative master chip in a Petri dish and further degassed until all

remaining air bubbles were removed. The PDMS was heated at 85 °C until cured (~20 min), and then peeled from the negative master; holes were punched through the reservoirs of the resulting PDMS chip to allow for the insertion of tubing. A thin PDMS film (substrate layer) was also made on a glass slide by spin-coating a 20:1 elastomer / curing agent mixture followed by curing. The substrate layer was then permanently bonded to the base of the microfluidic reactor (channel layer) after both components were exposed to oxygen plasma for 45 s. The resulting reactor (Figure 1) has a set channel depth of 150 μm and consists of a sinusoidal mixing channel 100 μm wide and a sinusoidal processing channel 200 μm wide, identical to the reactor described in previous publications from our group.

Flow Delivery and Control. Pressure-driven flow of liquids to the reactor inlet was provided using 1 mL gastight syringes (Hamilton, Reno, NV) mounted on syringe pumps (Harvard Apparatus, Holliston, MA). The microfluidic chip was connected to the liquid syringes *via* 1/16th-inch (OD) Teflon tubing (Scientific Products and Equipment, ON). Argon (Ar) gas flow was introduced to the chip *via* an Ar tank regulator and a downstream regulator (Johnston Controls) for fine adjustments. The chip was connected to the downstream regulator through a 1/16th-inch (OD) / 100-μm (ID) Teflon tube (Upchurch Scientific, Oak Harbor, WA). The liquid flow rate (Q_{liq}) was programmed *via* the syringe pumps and the gas flow rate (Q_{gas}) was fine-tuned *via* the downstream pressure regulator in order to set the nominal total flow rates (Q) of 50, 100, 200 and 400 μL/min described in the main text. Due to the compressible nature of the gas and the high gas/liquid interfacial tension, discrepancies arise between the nominal (programmed) and actual values of Q_{gas}, Q_{gas}/Q_{liq}, and the total flow rate (Q_{total}). Therefore, actual values of Q_{gas}, Q_{gas}/Q_{liq} and $Q_{total} = Q_{gas} + Q_{liq}$ for each microfluidic experiment (*Supporting Information*, Table S1) were calculated from the frequency of bubble formation and the average volume of gas bubbles,

determined from image analysis of the mean lengths of liquid and gas plugs, L_{liq} and L_{gas}, respectively, under a given set of flow conditions. This method of flow calculation has been previously described by our group.[21] For all experiments, the relative gas-to-liquid flow ratio, Q_{gas}/Q_{liq} ~1 and all actual Q_{total} values are within 10% of nominal Q values reported in the main text.

Visualization of the gas bubbles and liquid plugs within the microfluidic reactor was achieved using an upright optical microscope (Omax) with a 10× objective lens. Images were captured using a 2.07 megapixel PupilCam camera (Ken-A-Vision) and mean lengths of liquid and gas plugs were determined from the images using image analysis software (ImageJ).

Microfluidic Preparation of SN-38-PNPs. For microfluidic preparation of SN-38-PNPs, the following three fluid streams were combined to form gas-segmented liquid plugs within the reactor: (1) 1.0 wt % solution of PMCL-50, PMCL-75, or PMCL-100 in DMF with an SN-38/polymer (w/w) loading ratio of r = 0.75, (2) pure DMF, and (3) DMF/water. The flow rates of the three liquid streams were equal for all runs and the water content of the DMF/water stream was selected to yield steady state on-chip concentrations of 0.33 wt % copolymer and cwc + 10 wt % water, where cwc refers to the critical water contents of the three different copolymers (Table 1). For example, the critical water content of 0.33 wt % PMCL-75 in DMF was previously determined to be 9.4 wt %,[19] so that the steady state on-chip concentration of water for SN-38-PNP preparation from that copolymer was 19.4 wt %.

For each SN-38-PNP preparation, the sample was collected from the chip into vials containing 10× excess by volume of deionized water. In order to remove residual DMF, the resulting PNP dispersion was then dialyzed against deionized water for 12 hours with changing of water every hour for the first 4 h (6-8 kD MWCO dialysis membrane, Spectrum Laboratories).

Precipitated drug in the aqueous dispersion was removed by centrifugation at 16000×g for 18 minutes; the resulting supernatant containing PNP-encapsulated SN-38 was decanted into a pre-weighed vial. Deionized water was added to the centrifuge tube in order to rinse the residue and minimize loss of any SN-38-PNPs trapped in the pellet. Vortexing was applied for 5 min to the centrifugation tube in order to break up and re-suspend the pellet followed by another centrifugation step and collection of the supernatant. This rinsing process was repeated an additional two times. The masses of the PNP dispersion after collection, after dialysis, and after centrifugation and washing were weighed using an analytical balance and recorded for the encapsulation efficiency calculation. For each of the three copolymers, triplicate preparations (three separate batches) were carried out to assess reproducibility/variability.

Transmission Electron Microscopy. Negatively-stained samples for transmission electron microscopy (TEM) imaging were prepared by depositing a drop of SN-38-PNP dispersion on a carbon-coated 300-mesh copper TEM grid followed by a drop of 1 wt % uranyl acetate aqueous solution as a negative staining agent. Excess liquid was immediately removed using lens paper, followed by drying of the remaining liquid under ambient conditions. Imaging was performed on a JEOL JEM-1400 transmission electron microscope, operating at an accelerating voltage of 65 kV and equipped with a Gatan Orius SC1000 CCD camera. Mean sizes of spherical PNPs were determined by averaging average core sizes from three separate images of different regions of the TEM grid (N > 300 PNPs). Mean cylinder widths were determined from all visible cylinders (N = 10-50). Standard error (SE) on mean core size was calculated from the standard deviation (SD) of average core size from the three images: $SE = \frac{SD}{\sqrt{3}}$.

Dynamic Light Scattering. Effective hydrodynamic diameters and size distributions of SN-38-PNPs were determined from cumulant and CONTIN analysis, respectively, using dynamic

light scattering (DLS). CONTIN analysis provides a better representation of particle distributions than cumulent analysis given the broad nature of the distributions determined by TEM and the effect of gravimetric settling on DLS results. DLS measurements were carried out using a Brookhaven Instruments Zeta-Pals Analyzer equipped with a solid state laser (660 nm) with a maximum power output of 35 mW. All DLS measurements of SN-38-PNPs were performed in pure water and an experimental temperature of 25˚C and at a scattering angle of 90˚. Samples were diluted 4x with pure, filtered water and allowed to settle overnight before measurements. Hydrodynamic diameters were determined from average of most intense peak of CONTIN intensity distributions from three runs. Standard error (*SE*) on mean hydrodynamic diameters were calculated from the standard deviation (*SD*) of hydrodynamic diameters across triplicate preparations for each copolymer: $SE = \frac{SD}{\sqrt{3}}$.

SN-38 Encapsulation Efficiency Determination. High performance liquid chromatography (HPLC, Ultimate 3000, Thermo Scientific) equipped with a C18 column (Phenomenex Luna 5u C18) and a UV detector set at 265 nm was used to determine the drug loading efficiencies of SN-38-PNPs. The mobile phase, consisting of acetonitrile and water (65:35, v/v) was running at 1 ml/min. The mobile phase was adjusted to pH = 3 by formic acid to ensure SN-38 was in the closed lactone ring form during the assay. For each SN-38 sample, all of the water was removed by rotary evaporation at 25 °C followed by addition of pure acetonitrile to dissolve the solid. 50 μL of the resulting solution was then injected into the instrument and the UV detector reading of SN-38 in the sample was recorded. A calibration curve was made by analysis of 5 standards consisting of known concentrations of SN-38 in acetonitrile (5, 10, 20, 50, 100 ppm). All HPLC measurements were carried out at 25 °C.

Quantities of SN-38 in the various dissolved SN-38-PNP solutions were determined using

the calibration curve. Encapsulation efficiencies (*EE*) and drug loadings (*DL*) were calculated for each sample using the following equations:

$$EE\ /\ \% = \frac{mass\ encapsulated\ SN-38}{total\ mass\ SN-38} \times 100$$

$$r = \frac{total\ mass\ SN-38}{mass\ copolymer}$$

$$DL\ /\ \% = \frac{mass\ encapsulated\ SN-38}{mass\ encapsulated\ SN-38+mass\ copolymer} \times 100$$

$$DL\ /\ \% = \frac{r \times EE}{(r \times EE)+1} \times 100$$

Reported *EE* and *DL* values for each condition of *r* and *Q* were determined by averaging triplicate preparations using each copolymer, with reported standard error (*SE*) calculated from the standard deviation (*SD*) across the triplicate preparations: $SE = \frac{SD}{\sqrt{3}}$.

***In Vitro* SN-38 Release Kinetics.** Experiments were carried out to monitor the *in vitro* release of SN-38 from SN-38-PNPs using HPLC. In a typical experiment, a known mass (~2 g) of SN-38-loaded nanoparticles were put into a 5 mL Float-A-Lyzer tube (SpectrumLabs, MWCO 6-8 kDa) for each predetermined release time (t = 1, 2, 4, 8, 12, 18, 24 h). These tubes were then placed in a 5 L-beaker of the release medium, consisting of ~4 L of PBS; throughout release experiments, the release medium was constantly stirred using magnetic stirring and maintained at physiological temperature (37 ± 0.2°C). The infinite sink conditions are established by ensuring a large volume excess (2000×) between the sample and the PBS reservoir. In this way, the drug is strongly diluted once it crosses the membrane, such that an "infinite" chemical potential gradient is maintained throughout the release experiment.

At each predetermined time, one of the seven tubes was transferred to a vial and dried by rotary evaporation at 25 °C. Then a known quantity of acetonitrile was added to dissolve SN-38 and vortex was applied for 5 min to make sure all the SN-38 was dissolved. The concentration of the resulting solution was measured by HPLC (see previous section for specifications). Percentages of SN-38 released were calculated relative to determined masses of SN-38 in PNPs at the t = 0 release time. Reported release percentages at each time are averages of triplicate preparations using each copolymer, with reported standard error (*SE*) calculated from the standard deviation (*SD*) across the triplicate preparations: $SE = \frac{SD}{\sqrt{3}}$. The release profiles were fit to various models within XLFit, an add-in for Microsoft Excel, and the most appropriate fit was selected for each release profile. SN-38 release half times, $t_{1/2}$, were then determined from each fit, with an error calculated from the quality of the fit.

Results and Discussion

Table 2. Properties of SN-38-PNPs Prepared from Copolymers of Different MCL Contents

Copolymer	PMCL-50	PMCL-75	PMCL-100
d_h / nm[a]	260 ± 70	240 ± 40	270 ± 80
$d_{c,spheres}$ / nm[b]	22 ± 1	21 ± 1	19 ± 1
$w_{cylinders}$ / nm[b]	100 ± 30	130 ± 30	N/A
EE / %	3.0 ± 0.4	4.0 ± 0.6	2.7 ± 0.6
DL / %	2.2 ± 0.3	2.9 ± 0.4	2.0 ± 0.4
$t_{1/2}$ / h	3.4 ± 0.3	4.8 ± 0.9	6.2 ± 0.6

a) Determined from CONTIN analysis of DLS data
b) Determined from TEM size analysis

Sizes and Morphologies of SN-38-PNPs

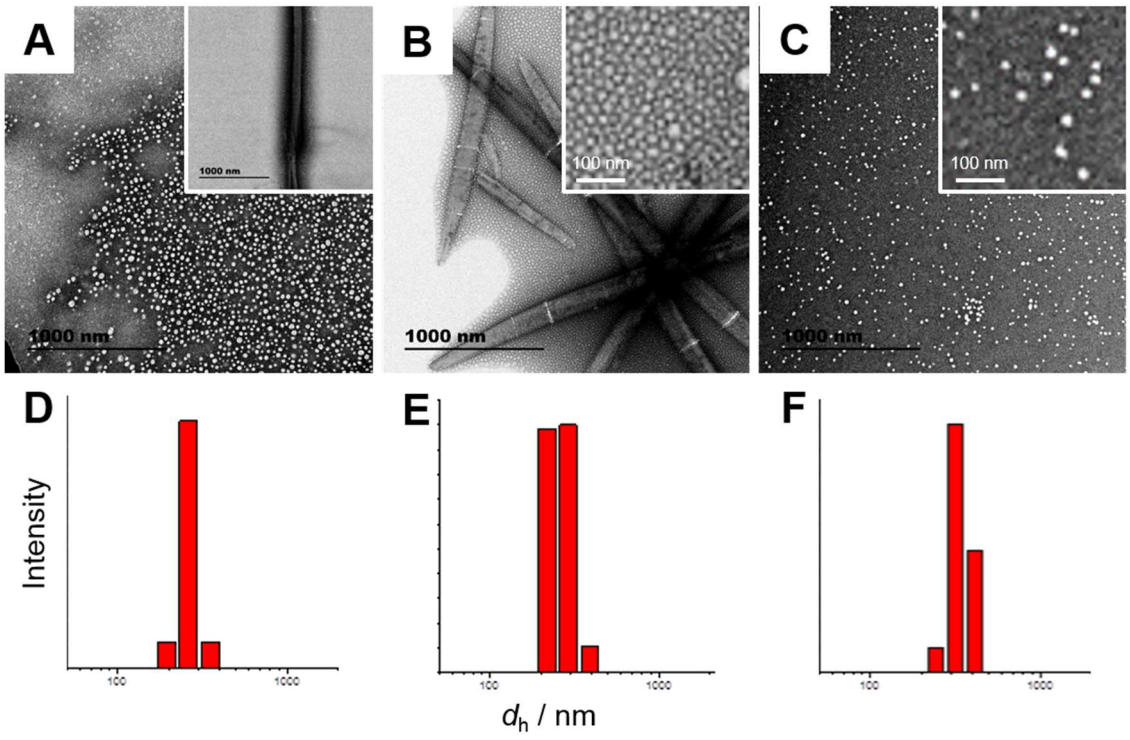

Figure 2. (A-B) Representative TEM images and (D-F) corresponding CONTIN intensity distributions of hydrodynamic diameters from DLS data of SN-38-PNPs prepared from PMCL-50 (A, D), PMCL-75 (B, E), and PMCL-100 (C, F).

SN-38-PNP preparations were analyzed by a combination of TEM and DLS to determine particle sizes and morphologies (Figure 2). TEM imaging of SN-38-PNPs was achieved by selective staining of PEO blocks with uranyl acetate so that PCL cores appear white in the resulting images (Figure 2, A-C). Numerous small spheres with a consistent mean core diameter of 20 nm were detected in all three samples. Along with the numerically dominant sphere populations in the TEM images, some long rodlike aggregates were present in PMCL-50 (Figure 2A, inset) and PMCL-75 (Figure 2B), but not in PMCL-100 (Figure 2C). Initial DLS experiments of the three dispersions gave rise to strong intermittent scattering such that reasonable autocorrelation functions could not be collected. Therefore, each sample was diluted with 4× filtered water and allowed to sit overnight to allow the largest aggregates in the dispersions to settle to the bottom of the vial before DLS measurements. This method gave rise to consistent autocorrelation functions from which CONTIN analysis yielded intensity distributions (Figure 2, D-F) with mean hydrodynamic diameters of ~250 nm for all three samples. The factor of 10 difference between spherical core sizes determined by TEM and hydrodynamic sizes determined by DLS is attributed to two factors. First, DLS sizes include the PEO coronae of micellar PNPs whereas only the PCL cores are visible by TEM. Second, TEM sizes are number-averaged quantities whereas mean DLS sizes are weighted according to the scattering intensity of dispersion fractions, which strongly favours larger aggregates in the distribution. The various SN-38-PNP dimensions measured by a combination of TEM and DLS are reported in Table 2.

These results show that a numerically dominant population of small spheres (~20 nm PCL cores), likely within the range of EPR activity,[3] is obtained irrespective of the MCL content within the hydrophobic core. Previous results with the same polymer series gave identical core sizes but with a narrower DLS population distribution yielding hydrodynamic diameters of ~60 nm.[19] This

suggests that the observed PNPs with 20 nm cores by TEM possess hydrated PEO shells that would place them well within the size regime of the EPR effect (50-100 nm).[3] The PCL core sizes are remarkably consistent for all three copolymers. This suggests that the relative lengths of the hydrophobic and hydrophilic blocks, which are constant for all three copolymers, is the most important factor in determining the sizes of the resulting spheres. Differences in the MCL content will effect small differences in the interfacial tension between the core and corona, which may be reflected in the small monotonic decrease in mean core size from 22 nm to 19 nm as the MCL content increases from 50% (PMCL-50) to 100% (PMCL-100). However, the small changes in core sizes suggest that these differences in interfacial tension are not large, likely due to the chemical similarity of MCL and CL repeat units. However, the MCL content does appear to influence the formation of longer rodlike aggregates, which are found in the PMCL-50 and PMCL-75 cases (Figure 2, A and B) but not in the PMCL-100 case (Figure 2C). Rodlike aggregate formation is known to be driven by core chain crystallization in PCL-based block copolymers.[29] Therefore, the TEM data suggests that the MCL content of PMCL-50 and PMCL-75 is not sufficient to completely disrupt PCL crystallization during self-assembly, allowing some rodlike aggregates to form. In contrast, in the PMCL-100 case every repeat unit contains a disruptive methyl group, precluding nucleation and growth of rodlike cylinders and leading to a population of pure spheres. We note that although the large rodlike aggregates found in PMCL-50 and PMCL-75 are well above the size regime for the EPR effect in drug delivery applications,[3] the consistent DLS result for all three samples after overnight settling suggests that these aggregates can be easily separated from the numerically dominant population of nanoscale spheres. Such separation of large rods from the PNP formulations would likely be necessary for delivery/targeting applications, since the large aggregates observed in Figure 2, A and B, may be too large to avoid opsonization

in the bloodstream.[3] However, an outstanding question is how the separation of large aggregates will affect the measured *EE* values. Since it is known that large aggregates are capable of solubilizing more drug than small aggregates due to their larger core volumes,[15] separation of rods could decrease the overall *EE* despite their relatively small number compared to spheres. These effects should be further quantified *en route* to possible drug delivery applications of these materials.

Since we did not study the SN-38-PNPs before quenching (dilution) and dialysis for this study, we do not know the extent to which the steps following collection from the chip affect the size and structure of the PNPs. The main objective here was to investigate the differences between the different hydrophobic block compositions and so keeping the preparation conditions identical (both before and after the microfluidic channel) was the most important feature of these experiments. However, our previous study showed that the same PMCL-50 copolymer formed PNPs on-chip at different flow rates without loaded drug with small but significant differences in sizes and morphologies immediately after collection from the chip (unquenched state), which were largely erased after quenching and dialysis.[19b] However, when the same copolymer was loaded with paclitaxel, flow-dependent differences in sizes and morphologies were observed even after dilution and dialysis.[19a] We conclude that the PMCL copolymers are dynamic due to a combination of low-T_g's and low crystallinities of the core-forming blocks, leading to changes in the size and structure of PNPs upon dilution and dialysis in the absence of drug. However, the presence of loaded drug appears to promote the retention of on-chip flow effects following dilution and dialysis, although the mechanism of this effect is currently uncertain.

Encapsulation Efficiency of SN-38-PNPs

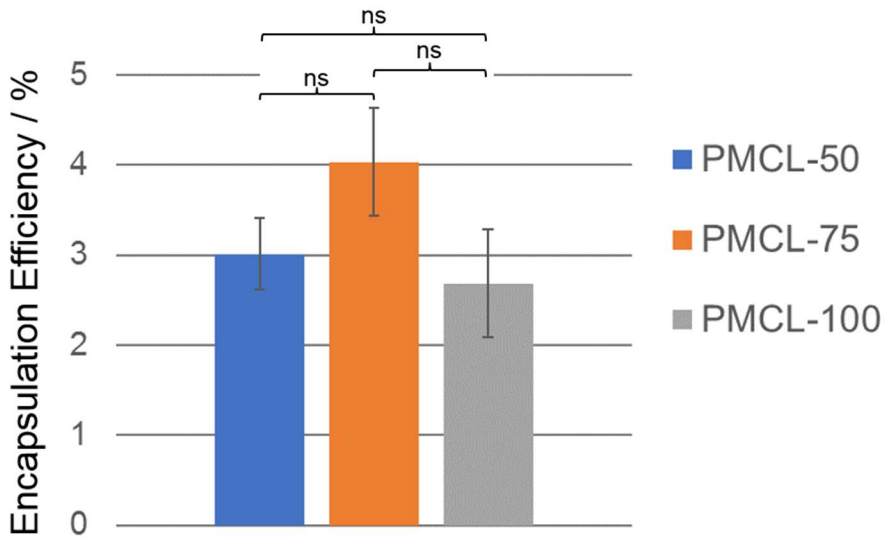

Figure 3. Mean SN-38 encapsulation efficiencies for SN-38-PNPs prepared from block copolymers with different MCL contents in the hydrophobic block. Statistical comparisons indicate no significant differences between *EE* values for different MCL contents.

Encapsulation efficiency is a critical parameter in drug delivery applications.[3] Increasing the encapsulation efficiency (*EE*) and drug loading level (*DL*) *via* chemical or processing strategies is an important goal in optimizing a nanomedicine formulation. Low drug load levels (*DL* = 1-5%) are typical of SN-38 encapsulation in aliphatic polyester-based PNPs, due to the low solubility of the drug molecules in the associated polymer cores during physical encapsulation.[11] In fact, the only block copolymer SN-38 nanomedicine that has completed phase III trials, NK012, relies on covalent attachment rather than physical encapsulation to entrap the drug within micellar PNPs of SN-38-conjugated poly(glutamic acid)-*block*-poly(ethylene oxide) (PGA-*b*-PEO).[4-6] However, methods to obtain high SN-38 loading levels *via* the simpler approach of physical encapsulation by increasing the solubility of the drug within the core-forming block, would certainly be desirable. Unfortunately, encapsulation efficiencies determined for all three copolymers were low (*EE* = 2.7-

4.0 %), with no significant differences between the different MCL contents (Figure 3). From this range of *EE* values, drug loading levels were also determined to be low (*DL* = 2.0 – 2.9 %), within the range typical of other block copolymer-based SN-38 nanomedicines. These results suggest that, although increasing the MCL content of the core has been shown to lower the core crystallinity,[19] it does not significantly increase the encapsulation of SN-38 within the cores of the resulting SN-38-PNPs. However, it is important to note that even low levels of SN-38 loading in block copolymer PNPs have shown promising *in vitro* and *in vivo* anticancer activity in other studies.[7-10, 12] Our finding that increasing the MCL content does not significantly increase SN-38 encapsulation is consistent with our earlier finding that increasing the MCL content also did not increase the encapsulation of PAX in the same series of copolymers.[19] Mean *EE* and *DL* values for SN-38 encapsulation in SN-38-PNPs prepared from the three copolymers are reported in Table 2.

***In Vitro* Drug Release Kinetics from SN-38-PNPs**

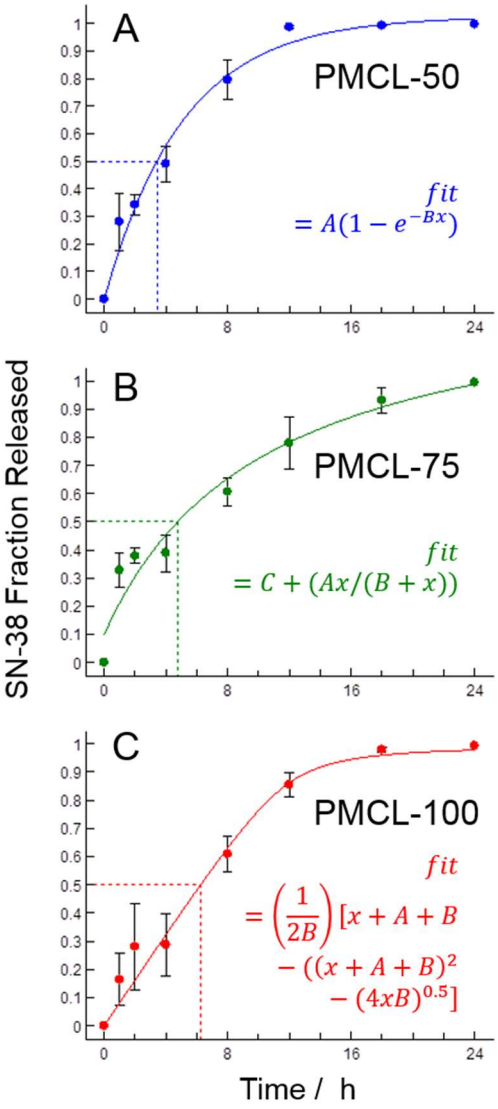

Figure 4. Mean *in vitro* release profiles for SN-38-PNPs prepared from block copolymers with different MCL contents in the hydrophobic block: A) PMCL-50, B) PMCL-75, and C) PMCL-100. Selected fits and associated fit equations are shown. Dashed lines indicate SN-38 release half times.

In vitro SN-38 profiles for SN-38-PNPs prepared from the three block copolymers are shown in Figure 4, along with associated fits and determinations of release half times, $t_{1/2}$. None of the three release profiles could be fit to the same mathematical model, indicating different

release kinetics for the three different copolymers. Moreover, $t_{1/2}$ values and associated errors determined from the fits show a monotonic increase with increasing MCL content (Figure 5), with statistical comparisons indicating a significant difference ($p < 0.005$) between release half times for the lowest (PMCL-50) and highest (PMCL-100) investigated MCL contents. Although more physically meaningful mathematical models could be more informative than the various polynomial models applied here, we have chosen to extract only a $t_{1/2}$ value from these data, in order to avoid over-interpreting a physical experiment designed for comparative purposes and which bears little resemblance to release in physiological systems.[17,18]

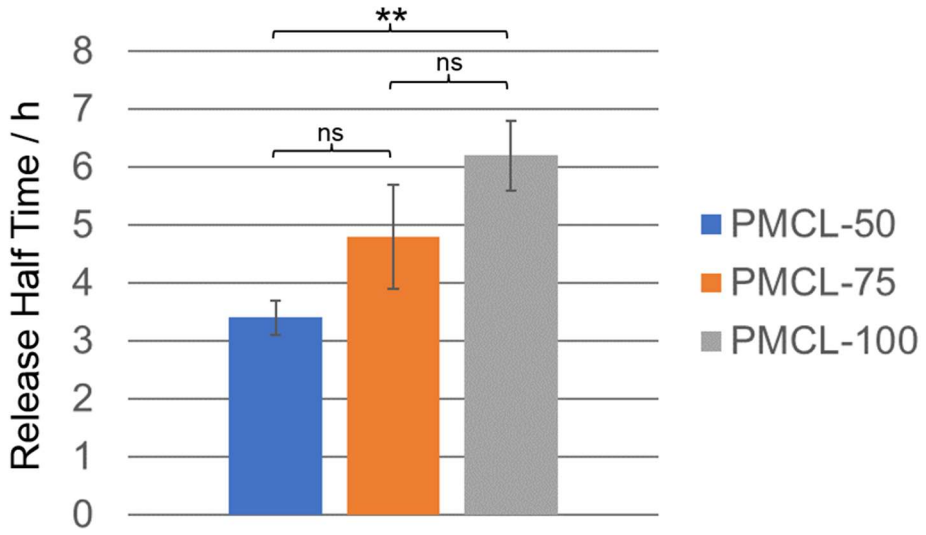

Figure 5. SN-38 release half times, $t_{1/2}$, for SN-38-PNPs prepared from block copolymers with different MCL contents in the hydrophobic block. Statistical comparisons between $t_{1/2}$ values are indicated with ** ($p < 0.005$) or ns ($p > 0.05$).

The increase in SN-38 release half times with increasing MCL content is in contrast to the statistically insignificant difference in PAX release kinetics reported recently using the same block copolymer series over the same change in MCL content.[19] The current marked effect of SN-38 release kinetics on MCL content may be due to changes in the spatial distribution of SN-38

molecules, as an increase in MCL content effects a decrease in the volume fraction of PCL crystallites within the hydrophobic core.[19] For example, within cores with higher crystallite fractions (PMCL-50), SN-38 may be forced to the core-corona interface by exclusion from the crystallites, leading to shorter diffusion distances for release and faster release kinetics. As the MCL content increases, the PCL crystallite fraction of the cores decreases, enabling a more uniform SN-38 distribution and leading to slower, more gradual release. It is important to note that the PNP samples in ref. 19 were prepared using the bulk method, which generally leads to faster release than microfluidic preparations due to slower mixing and greater partitioning of drug to the core-corona interface.[19] We believe that the greater extent of partitioning of the drug to the interface due to bulk preparation in ref. 19 overshadowed any differences due to the MLC content, explaining why similar differences in release half times were not found in the earlier study.

Conclusions

We have used a gas-liquid microfluidic reactor to prepare a series of SN-38-loaded PNPs from P(MCL-*co*-CL)-*b*-PEO copolymers with variable MCL content in the hydrophobic block. We show that all three copolymers form spheres with ~20 nm core diameters by TEM. Rigid rodlike aggregates were also formed by the PMCL-50 and PMCL-75 copolymers although DLS results suggest that these larger aggregates separate from the numerically predominant spheres by gravimetric sedimentation. SN-38 encapsulation efficiencies and loading levels were similar for the three copolymers, although we found that *in vitro* release kinetics became significantly slower as the MCL content increased. *In vitro* release kinetics represents an important figure of merit for drug delivery systems that could influence the bioavailability and biodistributions of SN-38 in future *in vivo* experiments. Therefore, the demonstrated ability to tune release half times *via*

controlled variation in the hydrophobic block composition, while at the same time maintaining constant PNP size and loading level, represents an intriguing chemical handle for the optimization of SN-38 nanomedicines. In addition, such fundamental insights into the effects of hydrophobic block composition on important figures of merit for drug delivery will hopefully provide design parameters for the future development of new polymers with optimized properties for SN-38 delivery. In a future report, we will combine this chemical handle with the shear processing handle arising from changes in flow rate within the microfluidic channels, along with exploring *in vitro* effects against cancer cells, further expanding our toolbox for polymeric SN-38 delivery.

Supporting Information. Sample HPLC chromatogram of SN-38; example of optical microscopy image of liquid plugs and air bubbles in microchannels; table of actual flow rates

Acknowledgements. We are grateful to the Natural Sciences and Engineering Research Council of Canada, NSERC, for financial support. We acknowledge Dr. Patrick Nahirney and the UVic EM lab (Department of Biology) for the continued use of their TEM.

References

1. Ebrahimnejad, P.; Dinarvand, R.; Sajadi, A.; Jaafari, M. R.; Nomani, A. R.; Azizi, E.; Rad-Malekshahi, M.; Atyabi, F. *Nanomedicine: NBM* **2010,** *6*, 478.

2. Bala, V.; Rao, S.; Boyd, B. J.; Prestidge, C. A. *J. Control. Release* **2013,** *172*, 48.

3. Elsabahy, M.; Wooley, K. L. *Chem. Soc. Rev.* **2012,** *41*, 2545.

4. Matsumura, Y. *Adv. Drug Deliver. Rev.* **2011,** *63*, 184.

5. Koizumi, F.; Kitagawa, M.; Negishi, T.; Onda, T.; Matsumoto, S.-i.; Hamaguchi, T.; Matsumura, Y. *Cancer Res.* **2006,** *66*, 10048.

6. Sumitomo, M.; Koizumi, F.; Asano, T.; Horiguchi, A.; Ito, K.; Asano, T.; Kakizoe, T.; Hayakawa, M.; Matsumura, Y. *Cancer Res.* **2008,** *68*, 1631.

7. Guo, Q.; Luo, P.; Luo, Y.; Du, F.; Lu, W.; Liu, S.; Huang, J.; Yu, J. *Colloids Surf. B* **2012,** *100*, 138.

8. Djurdjic, B.; Dimchevska, S.; Geskovski, N.; Petrusevska, M.; Gancheva, V.; Georgiev, G.; Petrov, P.; Goracinova, K. *J. Biomater. App.* **2015,** *29*, 867.

9. Lee, S.-Y.; Yang, C.-Y.; Peng, C.-L.; Wei, M.-F.; Chen, K.-C.; Yao, C.-J.; Shieh, M.-J. *Biomater.* **2016,** *86*, 92.

10. Lu, L.; Zheng, Y.; Weng, S.; Zhu, W.; Chen, J.; Zhang, X.; Lee, R. J.; Yu, B.; Jia, H.; Qin, L. *Colloids Surf. B* **2016,** *142*, 417.

11. Gan, M.; Zhang, W.; Wei, S.; Dang, H. *Artif. Cells Nanomed. Biotechnol.* **2017,** *45*, 389.

12. Dimchevska, S.; Geskovski, N.; Koliqi, R.; Matevska-Geskovska, N.; Vallejo, V. G.; Szczupak, B.; San Sebastian, E.; Llop, J.; Hristov, D. R.; Monopoli, M. P. *Int. J. Pharmaceut.* **2017,** *533*, 389.

13. Rychahou, P.; Bae, Y.; Reichel, D.; Zaytseva, Y. Y.; Lee, E. Y.; Napier, D.; Weiss, H. L.; Roller, N.; Frohman, H.; Le, A.-T. *J. Control. Release* **2018,** *275*, 85.

14. Oltra, N. S.; Nair, P.; Discher, D. E. *Annu. Rev. Chem. Biomol.* **2014,** *5*, 281.

15. Bains, A.; Cao, Y. M.; Moffitt, M. G. *Macromol. Rapid Comm.* **2015,** *36*, 2000.

16. Bains, A.; Cao, Y. M.; Kly, S.; Wulff, J. E.; Moffitt, M. G. *Mol. Pharm.* **2017,** *14*, 2595.

17. Letchford, K.; Liggins, R.; Wasan, K.; Burt, H. *Eur. J. Pharm. Biopharm.* **2009,** *71*, 196.

18. Bains, A.; Wulff, J. E.; Moffitt, M. G. *J. Colloid Interface Sci.* **2016,** *475*, 136.

19. a. Xu, Z.; Lu, C.; Lindenberger, C.; Cao, Y.; Wulff, J. E.; Moffitt, M. G. *ACS Omega* **2017,** *2*, 5289; b. Xu, Z. Control of Structure and Function of Block Copolymer Nanoparticles Manufactured in Microfluidic Reactors: Towards Drug Delivery Appplications. M.Sc. Thesis, University of Victoria, Victoria, Canada (2016).

20. Schabas, G.; Wang, C. W.; Oskooei, A.; Yusuf, H.; Moffitt, M. G.; Sinton, D. *Langmuir* **2008,** *24*, 10596.

21. Wang, C. W.; Oskooei, A.; Sinton, D.; Moffitt, M. G. *Langmuir* **2010,** *26*, 716.

22. Wang, C. W.; Sinton, D.; Moffitt, M. G. *J. Am. Chem. Soc.* **2011,** *133*, 18853.

23. Wang, C. W.; Bains, A.; Sinton, D.; Moffitt, M. G. *Langmuir* **2012,** *28*, 15756.

24. Wang, C. W.; Bains, A.; Sinton, D.; Moffitt, M. G. *Langmuir* **2013,** *29*, 8385.

25. Wang, C. W.; Sinton, D.; Moffitt, M. G. *ACS Nano* **2013,** *7*, 1424.

26. Bains, A.; Moffitt, M. G. *J. Colloid Interface Sci.* **2017,** *508*, 203.

27. Xu, Z. Q.; Yan, B.; Riordon, J.; Zhao, Y.; Sinton, D.; Moffitt, M. G. *Chem. Mater.* **2015,** *27*, 8094.

28. Xu, Z. Q.; Lu, C. H.; Riordon, J.; Sinton, D.; Moffitt, M. G. *Langmuir* **2016,** *32*, 12781.

29. Rizis, G.; van de Ven, T. G. M.; Eisenberg, A. *Soft Matter* **2014,** *10*, 2825.